ELSEVIER

Marine Geology 225 (2006) 247–263

MARINE GEOLOGY
INTERNATIONAL JOURNAL OF MARINE GEOLOGY, GEOCHEMISTRY AND GEOPHYSICS

www.elsevier.com/locate/margeo

Sediment compositions in offshore southern Taiwan and their relations to the source rocks in modern arc-continent collision zone

Jiun-Yee Yen [a,*], Neil Lundberg [b]

[a] *Center for Space and Remote Sensing Research, National Central University, No. 300, Jhongda Rd., Jhongli City, Taoyuan County 32001, Taiwan, ROC*

[b] *Department of Geological Sciences, Florida State University, 108 Carraway Building, Tallahassee, FL 32301, USA*

Received 7 March 2005; received in revised form 21 July 2005; accepted 2 September 2005

Abstract

Modal analyses of 31 sand samples collected by piston coring document variations in sediment composition along and across the developing collision zone off southern Taiwan and help constrain sediment transport paths and, by inference, of sediment sources. Overall, sand composition from this region is dominated by lithic-fragment populations, with a QtFL average of $Qt_{27}F_{21}L_{52}$. Three geographic domains are based on morphotectonics and variations in sand composition: (1) South China Sea and the adjacent slope of the accretionary prism; (2) suture zone south of southern Taiwan and north of the Luzon forearc; and (3) the Luzon forearc basin (North Luzon Trough) and immediate adjacent slopes. Sands from the accretionary prism and the suture zone contain subequal amounts of sedimentary and metamorphic lithic fragments ($Ls_{51}Lv_5Lm_{45}$ and $Ls_{47}Lv_5Lm_{48}$), respectively, whereas sands from the forearc basin are dominated by volcanic lithic fragments ($Ls_{29}Lv_{49}Lm_{22}$). In addition, compositions of individual sand beds vary dramatically in the forearc basin. This heterogeneity indicates that sediments from different sources have been deposited sequentially, but do not typically mix during transport and deposition. Similar, but less dramatic, within-core variations occur over the accretionary prism.

The major sediment input for the accretionary prism is from western Taiwan and is dominated by sedimentary and low-grade metamorphic lithic fragments. There appears to be a second sediment source, however, from southeastern China. This implies that a significant amount of sediment is the input from China to this region. The major component of sands in the suture zone is derived from Taiwan, but medium-grade metamorphic lithic fragments are rather sparse in these sands, considering the extensive and high-relief exposures of metamorphic rocks on the island of Taiwan. The major source of sands in the forearc basin is the active volcanoes of the Batan islands. Episodically, minor components appear to be fed to the forearc basin from the arcward slope of the accretionary prism, presumably by submarine mass wasting. This observation provides support for the hypothesized olistostromal origin for the Lichi Mélange of eastern Taiwan.

Keywords: Taiwan; arc-continent collision; modal analysis; source rocks; principal component analysis

1. Introduction

The relationship between sediment composition and plate tectonics has been the subject of intensive re-

* Corresponding author. Tel.: +886 3 4227151x57618; fax: +886 3 425 4908.
E-mail address: jyyen@csrsr.ncu.edu.tw (J.-Y. Yen).

0025-3227/$ - see front matter © 2005 Elsevier B.V. All rights reserved.
doi:10.1016/j.margeo.2005.09.003

search and discussion over the past two decades. Modal analysis by using framework compositional modes has been carried out by many groups to determine the provenance of sandstones and the effects of climate and weathering on sandstone composition, which has improved our knowledge about relationships between source area and mineralogy of sediments (e.g. Basu, 1976; Johnsson et al., 1991). Many tectonic settings have been studied extensively, producing generally accepted models of provenance relationships (Dickinson and Suczek, 1979; Ingersoll, 1990; Suttner and Basu, 1985).

Relatively few studies have been conducted to document the sediment composition in active, arc-continent collision zones (Abbott and Silver, 1990; Abbott et al., 1994; Dorsey, 1988; Findlay et al., 1995), yet this setting has been commonly inferred to explain the geologic history of ancient continental margins. Our knowledge of sedimentary processes and lithofacies trends in these tectonic settings is mainly based on ancient collision zones, especially on major continent–continent collisions (Hiscott et al., 1986; Ingersoll, 1988; Lash, 1987; Uddin and Lundberg, 2004). Important aspects of orogenic sedimentation, such as sediment composition, lithofacies distribution patterns, and sediment dispersal paths, have not been well documented in arc-continent collisional settings, especially in modern arc-continent collisional zones. At present, we lack a global model relating sediments to sediment sources and distribution paths in arc-continent collision settings. Arc-continent collisions provide an important mechanism for continental growth, with implications for distribution of valuable natural resources. Modal analysis of sands and sandstones can be useful in identifying potential source terranes and their tectonic settings.

Taiwan, as a relatively simple arc-continent collision, offers an opportunity to study active processes of collisional sedimentation. Our goal is to document the composition of sand beds in the Taiwan collision, focusing on modern marine sediments in the region south of Taiwan, where this collision is actively propagating. Moreover, the well-studied onland geology of Taiwan provides the potential both to track sediment sources and to make comparisons with earlier stages of the ongoing collision. The combination of modal analysis and principal component analysis used in this paper provides essential information indicating source areas and the distribution patterns of sediment, as well as distinguishing sediments that come from different tectonic settings. In addition, analyses of sand composition may serve to refine current models relating sediment composition to orogenic provenance types. Results can also be used to help understand the more mature segments of the collided arc-continent system. Specific objectives include documenting variations in sediment composition along and across the developing collision zone, and relating observed variations to inferred sediment sources and to sediment-dispersal paths.

2. Geologic background

The island of Taiwan is located along the boundary between the Philippine Sea and Eurasian plates, juxtaposed against the Asian continent (Fig. 1). Along this plate boundary, Taiwan marks the site where the polarity of subduction between these two plates is reversed: to the east and northeast, subduction of the Philippine Sea plate produces the Ryukyu island arc/Okinawa backarc trough, whereas to the south, subduction of the South China Sea along the Manila trench produces the Luzon island arc. Taiwan represents a modern, oblique collision between the west-facing Luzon arc and the Asian continental margin. This passive continental margin, developed during rifting in the mid-Tertiary, is made up of a rifted-margin sediment prism overlying thinned continental crust, which is now being deformed against the Luzon arc as it enters the Manila trench subduction zone. Detailed structural studies and plate reconstructions have shown that the arc-continent collision, which began in Miocene or earliest Pliocene time, is propagating southward (Sibuet and Hsu, 2004; Suppe, 1984; Teng, 1990). In northeasternmost Taiwan, in contrast, the Ilan plain is currently undergoing extension, possibly resulting from backarc extension in the Ryukyu system (Suppe, 1984; Teng, 1996).

The island of Taiwan is made up of three major north–south trending geologic provinces (Fig. 1). From west to east, these are the western Taiwan foredeep, the Central Mountains, and the Coastal Range. The western Taiwan foredeep consists of Plio-Pleistocene orogenic deposits that overlie older Tertiary sequences of the passive Chinese continental margin. Along the eastern portion of the foredeep, strata of both the upper collision-derived sequences and the underlying passive-margin deposits have been tectonically incorporated into the westward-advancing fold-and-thrust belt, forming the Western Foothills of the Taiwan mountain belt (Ho, 1982). Farther to the east, the western portion of the Central Ranges exposes low-grade metamorphosed Tertiary deposits (the Slate Formation), and the eastern flank of the Central Mountains exposes metamorphic complexes of the Yuli and Tai-

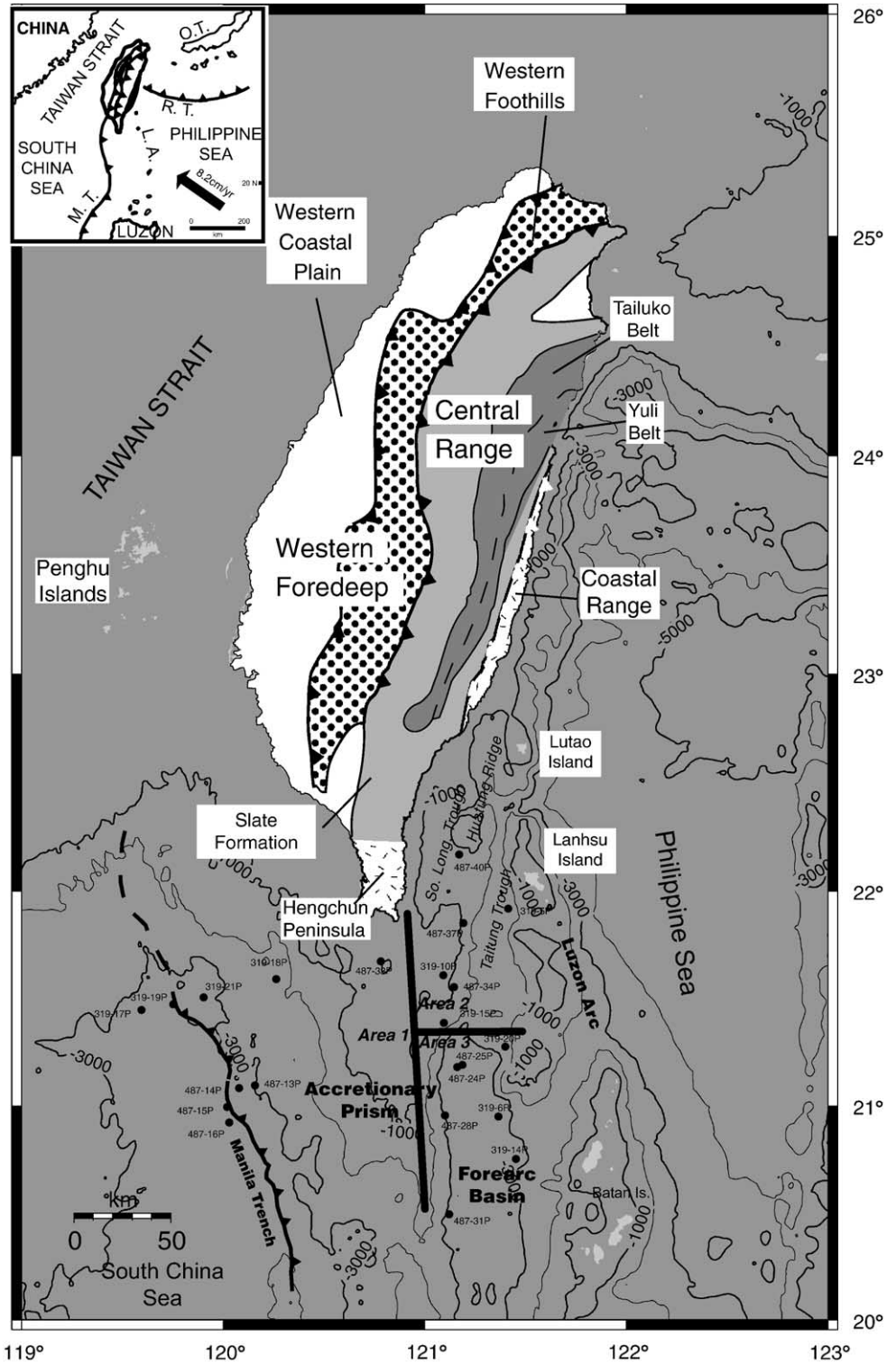

Fig. 1. Location, tectonic setting, simplified geology of Taiwan, and cores taken and morphotectonic regions (see detail in text).

luko Belts, which include pre-Tertiary rocks (Fig. 1). The rocks of the Central Mountains are complexly deformed and represent the northern extension of the accretionary wedge that lies east (arcward) of the Manila trench (Huang et al., 1992). The easternmost geologic belt of the island of Taiwan is the Coastal Range, a narrow strip of volcanic and sedimentary rocks representing the accreted island-arc terrane and its cover sequence. Miocene volcanic rocks of the Tuluanshan Formation comprise basal flows and a plutonic complex covered by thick agglomerates and tuffs. This basement unit is overlain by Plio-Pleistocene sedimentary rocks of the Takangko Formation, deposited in the collisional basin that formed in a setting analogous to that of the forearc basin, similar to the present-day North Luzon Trough to the south. Separating the Central Range from the Coastal Range is a remarkably linear, NNE-trending valley, the Longitudinal Valley, which is generally taken to represent the most obvious trace of the modern onland suture between deformed rocks of the Chinese continental margin and the accreted Luzon arc (Ho, 1982; Huang et al., 1992; Lundberg and Dorsey, 1988).

Uplift of about 5 mm/yr has been established in several areas of Taiwan by many workers with different approaches to measure uplift over a spectrum of time scales. Radiocarbon dating of uplifted corals in eastern, southeastern, and western coastal areas as summarized by Peng et al. (1977) shows consistent uplift at 5.0 ± 0.7 mm/yr over the past 9 ka. Work on corals by Wang et al. (1989), integrating U-series and radiocarbon dating with resurveying, suggests that Holocene uplift has been faster in eastern coastal areas (at 4 to 7 mm/yr) than in southernmost Taiwan (2 to 3 mm/yr). Fission-track dating in the Central Range has yielded high cooling rates for the late Quaternary (Liu, 1982), rates that Barr and Dahlen (1990) have shown to be consistent with a modern denudation rate of 5.5 mm/yr (Li, 1976), on the basis of heat-flow constraints and thermal modeling of the mountain belt. In general, aside from central and southern portions of the coast of eastern Taiwan, which has uplift rates of 9–10 mm/yr, most of the coasts around Taiwan show an average uplift rate of 5 mm/yr. The coast in the southwestern Taiwan of Pingtung country exhibit an anomalous high subsidence rate of 6–8 mm/yr in the Holocene (Liew et al., 2004). In addition, unroofing rates of 4 to 5 mm/yr have been calculated by Dorsey (1988) for the ancestral Central Range of Taiwan during the Pliocene to earliest Pleistocene, on the basis of the first appearance (1.4 Ma) of orogenic detritus derived from biotite-grade rocks that were metamorphosed at 425 ± 75 °C and 4 kbar (Ernst, 1983) during the ongoing collision. Repeated geodetic surveys during 1984 to 1987 by Liu and Yu (1990) revealed that Coastal Range is being uplifted with respect to the Longitudinal Valley at a rate of about 30 mm/yr, although this rate is only found in a very confined region. Liu and Yu (1990) also concluded that the coast of eastern Taiwan is undergoing uplift at a rate ranging from 0 to 35 mm/yr. Lundberg and Dorsey (1990) obtained an average uplift rate of 7.5 and 5.9 mm/yr over the past 1 my from a thick sequence of orogenic strata exposed in the Coastal Range that represent relative maxima in total uplift of the region.

3. Sampling and analytical methods

Samples analyzed in this research were selected from piston cores that were collected on Cruise OR487 of the *R/V Ocean Researcher 1*, during May 13 to 24, 1997, and Cruise OR-319, also by the *R/V Ocean Researcher 1*. Locations of cores are also shown in Fig. 1. Table 1 lists the samples taken from each core. Samples for this study were taken from the available sand beds from the piston cores.

For modal analysis of sands and silts, sediments were sieved to isolate the size fraction >63 μm, which were epoxied into artificial aggregates for thin-section preparation. Thin sections were stained for feldspars, preserving half of each section for detailed textural studies and for improved lithic identification. Samples were point-counted following the Gazzi-Dickinson convention (Dickinson, 1970) in order to minimize effects of grain-size variation on sand composition (Ingersoll et al., 1984). At least 300 grains were counted in. Table 2 presents the classification of grain types and recalculated parameters used in this research. Conventions for grain recognition followed those of Dickinson (1970), Graham et al. (1976), Ingersoll and Suczek (1979), and Dorsey (1988). Normalized results of our sand modal analysis are listed in Table 3. Modal sand compositions were plotted on standard ternary diagrams (QtFL and others) in order to evaluate the nature of sediment-source terranes.

In order to subjectively classify the samples on the basis of different compositional properties without biased by any previous geologic knowledge of the area, or conjecture the source areas before analyzing the data, we applied principal component analysis to the detrital modal data collected on sand. Principal component analysis is a mathematical method for assessing variable groupings within multivariate data. The method takes n variables and finds "components or indices" that are uncorrelated and explain a certain proportion of the total variability in the data. The method reduces the

Table 1
Localities of cores and samples analyzed from offshore southern Taiwan

Core number	Latitude	Longitude	Water depth (m)	Sample number	Morphotectonic domain[a]
487-13P	21°03.94′	120°07.63′	3525	JY10, JY12, JY14	1
487-14P	21°03.22′	120°03.01′	3221	JY23	1
487-15P	20°58.01′	119°59.53′		JY16, JY17, JY18, JY20, JY28	1
487-16P	20°53.74′	120°00.15′		JY32, JY36	
487-24P	21°09.0′	121°06.47′	3453	JY78, JY175	3
487-25P	21°09.6′	121°07.98′	3384	JY100	3
487-28P	20°55.7′	121°02.91′	3601	JY95, JY106, JY109, JY112	3
487-31P	20°28.49′	121°04.14′	2780	JY130	3
487-33P	21°38.08′	120°44.24′	492	JY136	1
487-34P	21°31.01	121°05.52	867	JY153	
487-37P	21°48.63′	121°08.26′	803	JY149	2
487-40P	22°07.49	121°07.02	1267	JY156, JY157	2
319-5P	21°52.61′	121°21.30′	2795	JY200	2
319-6P	20°55.38′	121°18.45′	3612	JY201	3
319-10P	21°34.28′	121°02.41′	909	JY202	2
319-14P	20°43.71′	121°23.55′	3562	JY203	3
319-15P	21°21.16′	121°02.59′	1824	JY204	2
319-17P	21°24.72′	119°34.61′	3060	JY205	1
319-18P	21°33.20′	120°13.81′	2873	JY206	1
319-19P	21°26.30′	119°43.85′	3294	JY207	1
319-20P	21°14.62′	121°20.46′	3267	JY208	3
319-21P	21°28.18′	119°52.70′	3103	JY209	1

[a] See text for description.

dimensions (and complexities) of the original data set to the extracted uncorrelated indices (called components). These indices are in effect "dimensions" within the data that explain the data in fewer variables than the original number. We used a *varimax* rotation method which rotate the reference frame to obtain rotated component loadings in order to recover maximum variabilities in sample sets. Data obtained from sand analysis were first recalculated and normalized, and a data matrix was constructed. Rows of this matrix represent compositional parameters and columns represent individual samples. The SPSS package for Windows was used to perform Q-mode principal component analysis (in which vectors represent samples, rather than compositional variables). The purposes of the Q-mode analysis are: (1) to find the minimum number of "end-members" defined by the sample population; (2) to describe the relationships between end-members and the samples; and (3) to specify the compositions of the end-members in relationship to the compositions of samples. The number of end-members is determined by how much original variation is retained when an end-member is extracted. If the amount of information or variation is trivial to the solution, the end-member is taken as being insignificant.

Table 2
Recalculated sandstone modal parameters used in this study

(1) Primary parameters (after Graham et al., 1976; Dickinson and Suczek, 1979; Dorsey, 1988)

Qt=Qm+Qp, where
- Qt=total quartzose grains
- Qm=monocrystalline quartzose grains
- Qp=polycrystalline quartz grains, including chert grains

F=P+K, where
- F=total felldspar grains
- P=plagioclase feldspar grains
- K=potassium feldspar grains

L=Ls+Lv+Lm=Lsm+Lvm=Ls+Lv+Lm_1+Lm_2=Lt−Qp, where
- Ls+sedimentary lithic fragments, mostly mudstones and shales
- Lv=volcanic lithic fragments
- Lm=metamorphic lithic fragments
- Lsm=sedimentary and metasedimentary lithic fragments
- Lvm=volcanic, hypabyssal, metavolcanic lithic fragments
- Lm_1=very low- to low-grade metamorphic lithic fragments
- Lm_2=low- to intermediate-grade metamorphic lithic fragments
- Lt=total aphanitic lithic fragments

(2) Secondary parameters (after Dickinson, 1970)

P/F=plagioclase/total feldspar grains
Lv/L=volcanic/lithic fragments

4. Analytical results

4.1. Sand petrology

Sand samples collected from south of Taiwan are generally rich in lithic fragments, with lesser and sub-

Table 3

Sample	QpLvmLsm %			QpLvLs %			QtFL %			QmFLt %			QmPK %			$LsLm_1Lm_2$ %			LsLvLm %			$LsLvLm_1$ %			$LsLvLm_2$ %		
	Qp %	Lvm %	Lsm %	Qp %	Lv %	Ls %	Qt %	F %	L %	Qm %	F %	Lt %	Qm %	P %	K %	Ls %	Lm_1 %	Lm_2 %	Ls %	Lv %	Lm %	Ls %	Lv %	Lm_1 %	Ls %	Lv %	Lm_2 %
JY32-Area 1	0.0	4.9	95.1	0.0	7.7	92.3	7.1	19.6	73.2	7.1	19.6	73.2	33.3	0.0	66.7	61.5	38.5	0.0	58.5	4.9	36.6	58.5	4.9	36.6	92.3	7.7	0.0
JY28-Area 1	2.3	7.5	90.2	3.1	10.3	86.6	14.9	18.5	66.7	13.3	18.5	68.2	46.4	53.6	0.0	70.0	29.2	0.8	64.6	7.7	27.7	65.1	7.8	27.1	88.4	10.5	1.1
JY23-Area 1	8.3	5.6	86.1	13.2	8.8	77.9	19.0	18.4	62.7	13.3	18.4	68.4	47.7	34.1	18.2	57.0	43.0	0.0	53.5	6.1	40.4	53.5	6.1	40.4	89.8	10.2	0.0
JY20-Area 1	8.2	0.8	91.0	15.2	1.5	83.3	22.9	13.1	64.0	17.1	13.1	69.7	56.6	30.2	13.2	49.5	43.2	7.2	49.1	0.9	50.0	52.9	1.0	46.2	85.9	1.6	12.5
JY18-Area 1	2.3	15.1	82.6	3.5	22.8	73.7	11.9	21.4	66.7	10.3	21.4	68.3	37.1	14.3	48.6	59.2	40.8	0.0	50.0	15.5	34.5	50.0	15.5	34.5	76.4	23.6	0.0
JY17-Area 1	0.9	2.8	96.3	1.5	4.5	94.0	9.9	23.6	66.5	9.3	23.6	67.1	30.0	26.0	44.0	60.6	32.7	6.7	58.9	2.8	38.3	63.0	3.0	34.0	86.3	4.1	9.6
JY16-Area 1	5.5	0.6	93.9	10.4	1.0	88.5	24.3	11.6	64.0	20.6	11.6	67.8	67.9	14.8	17.3	50.0	42.4	7.6	49.7	0.6	49.7	53.8	0.6	45.6	85.9	1.0	13.1
JY14-Area 1	13.0	0.0	87.0	34.8	0.0	65.2	21.8	9.8	68.4	11.5	9.8	78.6	60.0	33.3	6.7	28.1	71.9	0.0	28.1	0.0	71.9	28.1	0.0	71.9	100.0	0.0	0.0
JY12-Area 1	17.9	0.0	82.1	45.5	0.0	54.5	33.3	26.3	40.4	24.6	26.3	49.1	53.8	30.8	15.4	26.1	73.9	0.0	26.1	0.0	73.9	26.1	0.0	73.9	100.0	0.0	0.0
JY10-Area 1	5.1	3.8	91.0	7.3	5.5	87.3	16.0	24.8	59.2	12.8	24.8	62.4	37.2	46.5	16.3	67.6	32.4	0.0	64.9	4.1	31.1	64.9	4.1	31.1	94.1	5.9	0.0
319-21P-Area 1	14.8	0.8	84.4	25.7	1.4	73.0	43.3	4.3	52.4	34.1	4.3	61.5	89.9	3.8	6.3	50.0	42.6	7.4	49.5	0.9	49.5	53.5	1.0	45.5	85.7	1.6	12.7
319-19P-Area 1	16.1	4.3	79.6	28.3	7.5	64.2	52.4	6.8	40.8	44.5	6.8	48.7	87.6	8.2	4.1	45.9	47.3	6.8	43.6	5.1	51.3	46.6	5.5	47.9	79.1	9.3	11.6
319-18P-Area 1	6.4	2.0	91.6	12.3	3.8	83.8	25.6	3.6	70.8	20.8	3.6	75.6	87.3	8.9	3.8	47.4	43.9	8.7	46.4	2.1	51.5	50.7	2.3	47.0	81.3	3.7	14.9
319-17P-Area 1	12.8	6.8	80.3	23.8	12.7	63.5	48.5	9.1	42.3	42.3	9.1	48.5	83.6	5.7	10.7	42.6	45.7	11.7	39.2	7.8	52.9	44.0	8.8	47.3	67.8	13.6	18.6
JY136-Area 1	6.1	8.5	85.4	6.7	9.3	84.0	20.5	10.7	68.8	16.1	10.7	73.2	62.1	37.9	0.0	90.0	10.0	0.0	81.8	9.1	9.1	81.8	9.1	9.1	90.0	10.0	0.0
Mean	8.0	4.2	87.8	15.4	6.5	78.1	24.8	14.8	60.4	19.9	14.8	65.4	58.7	23.2	18.1	53.7	42.5	3.8	50.9	4.5	44.6	52.8	4.6	42.5	86.9	6.9	6.3
S.D.	5.7	4.1	5.4	13.4	6.1	11.9	13.8	7.5	11.1	11.7	7.5	9.7	20.8	16.5	19.6	16.1	15.4	4.3	14.2	4.3	16.5	14.0	4.3	16.1	8.5	6.4	7.1
JY157-Area 2	7.5	0.0	92.5	17.8	0.0	82.2	20.3	18.4	61.3	15.4	18.4	66.2	48.7	33.0	18.3	37.2	45.7	17.0	237.2	0.0	62.8	44.9	0.0	55.1	68.6	0.0	31.4
JY149-Area 2	25.9	2.7	71.4	42.7	4.5	52.8	36.9	29.9	33.2	25.3	29.9	44.8	51.2	21.6	27.2	44.8	30.5	24.8	243.1	3.7	53.2	56.6	4.8	38.6	61.0	5.2	33.8
319-5P-Area 2	14.0	5.6	80.4	25.3	10.1	64.6	31.1	17.2	51.7	22.7	17.2	60.1	60.0	26.7	13.3	44.3	39.1	16.5	41.5	6.5	52.0	49.0	7.7	43.3	65.4	10.3	24.4
319-15P-Area 2	15.0	4.2	80.8	22.5	6.3	71.3	49.6	9.6	40.8	42.4	9.6	48.0	83.5	11.0	5.5	58.8	28.9	12.4	55.9	4.9	39.2	63.3	5.6	31.1	77.0	6.8	16.2
319-10P-Area 2	24.8	6.9	68.3	32.5	9.1	58.4	51.8	13.6	34.5	40.5	13.6	45.9	76.7	17.2	6.0	65.2	27.5	7.2	59.2	9.2	31.6	63.4	9.9	26.8	78.9	12.3	8.8
Mean	17.4	3.9	78.7	28.2	6.0	65.8	37.9	17.7	44.3	29.2	17.7	53.0	64.0	21.9	14.1	50.1	34.3	15.6	47.4	4.9	47.8	55.4	5.6	39.0	70.2	6.9	22.9
S.D.	7.8	2.7	9.5	9.7	4.0	11.4	13.1	7.6	12.0	11.7	7.6	9.6	15.4	8.5	9.0	11.5	7.8	6.5	9.6	3.4	12.3	8.4	3.7	11.1	7.6	4.8	10.5
JY95-Area 3	0.0	0.0	100.0	0.0	0.0	100.0	35.1	35.1	29.8	35.1	35.1	29.8	57.1	34.3	8.6	35.3	64.7	0.0	35.3	0.0	64.7	35.3	0.0	64.7	100.0	0.0	0.0
JY78-Area 3	2.3	7.5	90.2	3.1	10.3	86.6	14.9	18.5	66.7	13.3	18.5	68.2	46.4	53.6	0.0	70.0	29.2	0.8	64.6	7.7	27.7	65.1	7.8	27.1	88.4	10.5	1.1
JY175-Area	327.0	9.5	63.5	33.3	11.8	54.9	57.3	17.8	24.9	48.1	17.8	34.1	76.7	8.6	14.7	70.0	30.0	0.0	60.9	13.0	26.1	60.9	13.0	26.1	82.4	17.6	0.0
JY130-Area 3	15.3	26.4	58.3	19.0	32.8	48.3	20.6	36.2	43.3	12.8	36.2	51.1	27.3	54.5	18.2	66.7	28.6	4.8	45.9	31.1	23.0	47.5	32.2	20.3	57.1	38.8	4.1
JY112-Area 3	5.6	52.1	42.3	6.7	61.7	31.7	12.9	36.4	50.8	9.8	36.4	53.8	22.8	61.4	15.8	63.3	26.7	10.0	28.4	55.2	16.4	29.7	57.8	12.5	32.2	62.7	5.1
JY109-Area 3	3.9	80.6	15.6	4.3	89.0	6.7	14.4	37.8	47.8	12.4	37.8	49.7	29.6	50.7	19.7	39.3	57.1	3.6	6.4	83.8	9.8	6.4	84.3	9.3	7.0	92.4	0.6
JY106-Area 3	8.2	73.8	18.0	9.4	84.9	5.7	13.9	34.3	51.9	9.3	34.3	56.5	24.4	65.9	9.8	27.3	72.7	0.0	5.4	80.4	14.3	5.4	80.4	14.3	6.3	93.8	0.0
JY100-Area 3	22.2	14.3	63.5	33.3	21.4	45.2	36.4	25.6	38.0	25.6	25.6	48.8	55.9	18.6	25.4	47.5	52.5	0.0	38.8	18.4	42.9	38.8	18.4	42.9	67.9	32.1	0.0
319-6P-Area 3	6.5	72.0	21.5	6.9	77.0	16.1	17.8	41.3	40.8	15.0	41.3	43.7	27.8	59.1	13.0	70.0	25.0	5.0	16.1	77.0	6.9	16.3	77.9	5.8	17.1	81.7	1.2
319-20P-Area 3	13.4	68.3	18.3	14.7	74.7	10.7	33.3	21.2	45.5	26.3	21.2	52.6	59.4	39.1	1.4	53.3	40.0	6.7	11.3	78.9	9.9	11.4	80.0	8.6	12.3	86.2	1.5
319-14P-Area 3	3.4	93.1	3.4	3.5	94.7	1.8	18.5	36.3	45.2	16.9	36.3	46.8	34.4	60.7	4.9	50.0	50.0	0.0	1.8	96.4	1.8	1.8	96.4	1.8	1.8	98.2	0.0
Mean	9.8	45.2	45.0	12.2	50.7	37.1	25.0	30.9	44.0	20.4	30.9	48.6	42.0	46.0	12.0	53.9	43.3	2.8	28.6	49.3	22.1	28.9	49.8	21.2	42.9	55.8	1.2
S.D.	8.7	34.2	32.4	11.8	35.9	33.5	13.9	8.5	11.2	12.2	8.5	10.4	18.1	18.7	7.9	15.3	16.9	3.5	22.4	35.8	18.3	22.5	36.0	18.6	37.1	37.0	1.8

equal amounts of quartz and feldspar grains. The modal average of total quartz, feldspar, and lithic fragments is $Qt_{27}F_{21}L_{52}$. Texturally, most grains range from fine sand to very fine sand, with the exception of volcanic lithic fragments, which range from medium to very fine sand, and locally medium-sand sized fragments of slate and/or siltstone are present. Grain shape (roundness/angularity) varies between contrasting grain types. Mudstone and shale fragments are rounded to sub-rounded, with rather vague grain boundaries (Fig. 2A,B). Slate and schist fragments generally appear elongated (acicular or tabular) in shape, ranging from sub-rounded to sub-angular (Fig. 2C). Volcanic lithic fragments range from angular to sub-rounded (Fig. 2D). Diagenetic effects are minimal in all the samples studied, and only relatively few grains, typically volcanic lithic fragments, suffer from severe alteration.

Compositional variations are clearly related to morphotectonic settings of the core locations, and serve to define distinct petrofacies. On the western side of the accretionary prism, sands contain relatively more abundant sedimentary and low-grade metamorphic lithic fragments. On the eastern side of the accretionary prism, however, sand compositions are more complex. Samples from the northern part of the eastern side of the accretionary prism typically contain medium-grade metamorphic lithic fragments, whereas samples from the southern part (in and near the forearc basin) are distinguished by the presence of abundant volcanic lithic fragments. This observation serves to divide the study area geographically into three different petrotectonic provinces (Fig. 1). The crest of the accretionary prism domains roughly along the 121°E meridian serves to separate the eastern domains from the western domain. A line drawn along 21°20′N serves to further divide two distinct eastern domains. Although the northern part of the eastern domains represents several different geological elements, the relatively small number of sand samples recovered from this area limits our ability to further divide this area. We have labeled these three domains *area 1* (western), *area 2* (northeastern), and *area 3* (southeastern). Area 1 represents the frontal portion of the accretionary prism and the region immediately west of the Manila trench. Area 2 represents the submarine portion of the suture zone, and includes the Southern Longitudinal Trough (offshore extension of the Longitudinal Valley); the Huatung Ridge (offshore extension of the Coastal Range, including the Lichi mélange), and the Taitung trough (a steep-sided depression separating the Huatung Ridge and Luzon Arc). Area 3 is the forearc basin and the immediately adjacent rear (eastern) slope of the accretionary prism (Fig. 1). In addition, sands from a single core, Core OR487-33P, are compositionally unique (very rich in siltstone fragments) and do not fit into any of the petrofacies defined by sands from the three domains. This core was collected

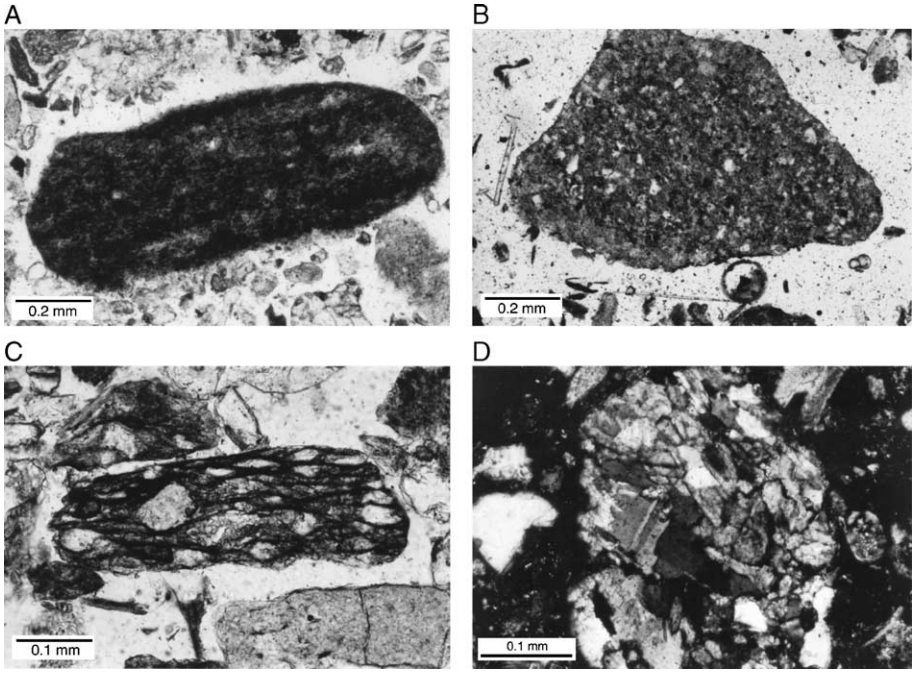

Fig. 2. Photomicrographs of selected samples (cross-polarized light). (A) Shale fragment. (B) Siltstone fragments. (C) Volcanic lithic fragments. (D) Low-grade metamorphic lithic fragments.

from the crest of the accretionary prism just south of the southern tip of Taiwan (Fig. 1).

The average of total lithic fragments in all samples is 52%, with 63% in area 1, 46% in area 2, and 39% in area 3. The remainder of the sand is composed mostly of quartz and feldspar, with minor heavy minerals and intrabasinal grains. The QtFL modal average of area 1 sand is $Qt_{25}F_{15}L_{60}$, the average of area 2 is $Qt_{38}F_{18}L_{44}$, and the average of area 3 is $Qt_{25}F_{31}L_{44}$.

4.1.1. Results of sand petrology

Sands in area 1 and area 2 generally lack significant amounts of feldspar grains, suggesting the lack of input from igneous and basement sources for these two areas (Fig. 3A). In contrast, area 3 contains more abundant feldspar grains and relatively less quartz. The modal averages of area 1 and area 2 (Fig. 3B) fall into the provenance field defined by Teng (1979) in his study of sandstones from the Coastal Range of Taiwan as "type 3", lithic arenites that contrast with strongly volcaniclastic ("type 1") and highly quartzose ("type 2") sandstones. These sands also plot in Ingersoll and Suczek (1979) "suture zone" provenance field. In contrast, the mean of area 3 sands plots in Dickinson (1985) provenance field of magmatic arc.

The offshore Taiwan sands we analyzed contain very little polycrystalline quartz, and so data plot very similarly on QmFLt and QtFL plot (Fig. 3C). In contrast, the provenance field determined by Dickinson and Suczek (1979) to represent "recycled orogens" shifts dramatically to the Lt pole of the QmFLt diagram. Data from areas 1 and 2 plot within the "recycled orogen".

Sands data from area 1 and area 2 plot in overlappng regions near the Qm pole of a QmPK diagram (Fig. 3D), with area 1 sands showing much greater variability. The compositions of these two groups are essentially indistinguishable in this plot. Value for area 3 plot close to the middle of the Qm-P join. Variations in the light, monocrystalline components, however, are of secondary importance in the interpretation of Taiwan sands.

The QpLvmLsm plot is useful for differentiating magmatic-arc from recycled-orogen provenance. Compositions of sands from area 1 and area 2 plot in the tight cluster near the Lsm pole of this diagram (Fig. 3E). Sands from area 3, in contrast, plot between Lvm and Lsm with a small amount of Qp. Although the mean of area 3 sands plots near the center of the Lvm–Lsm join, the individual data points stretch from the Lvm pole to the Lsm pole, consistent with a mixed provenance.

On an LmLvLs diagram, data from areas 1 and 2 plot along the middle of the Lm–Ls join, with very few volcanic lithic fragments (Fig. 3F). The two areas plot on top of each other, with area 2 sands showing somewhat less variability than do sands from area 1. The modal average of area 3 is located near the middle of the triangle. The data points of area 3 sands are distributed from very near the Lv pole to the midpoint of the Ls–Lm join, indicating a mixed provenance.

Dorsey (1988) introduced the $LsLm_1Lm_2$ plot to differentiate the grade of metamorphism of source rocks of phyllarenitic suites. Data from this research plot along the mid-point of the Ls–Lm_1 join (Fig. 3G). Sands from both area 1 and area 3 lack medium-grade metamorphic lithic fragments. Sands from area 2 contain relatively more medium-grade metamorphic lithic fragments consistent with the location of closer to the eastern flank of the Central Range. The ratio of Lm_1 to Ls is about the same for all three areas, at about 1:1.

Area 3 sands contain very few medium-grade metamorphic lithic fragments, so their values plot very close to the Ls–Lv join of the $LsLvLm_2$ diagram, with a large standard deviation that stretches from near the Ls pole nearly to the Lv pole (Fig. 3H). Unlike sands of area 3, those of areas 1 and 2 contain very few volcanic lithic fragments. Sands from area 2 stand out from those from area 1 by containing more abundant medium-grade metamorphic lithic fragments. The individual data points show minor overlap between their respective fields as defined by area.

4.2. Principal component analysis of sand compositions

We carried out Q-mode principal component analysis on the modal data set we produced on the sands from offshore southern Taiwan. Initially, we included all the samples in the analysis and extracted four components for the entire data set. Relative loadings (or component scores) were then assigned to each sample, representing the contributions of each of the four end-members to that sample. Higher loadings indicate that a sample has a relatively high contribution of the respective component. Negative loadings are also statistically possible, suggesting that a sample has a negative contribution from the respective component. In fact, the results of Q-mode principal component analysis on our entire data set yielded many negative loadings. Although negative component loadings are meaningful statistically, they are less helpful in interpreting relationships between samples and potential sources. The relative abundance of negative compositional loadings yielded by our initial analysis may be an indication that the characteristics of sediments in one area (or basin) are not directly related to samples in neighboring areas (or basins). This may reflect morphotectonic barriers,

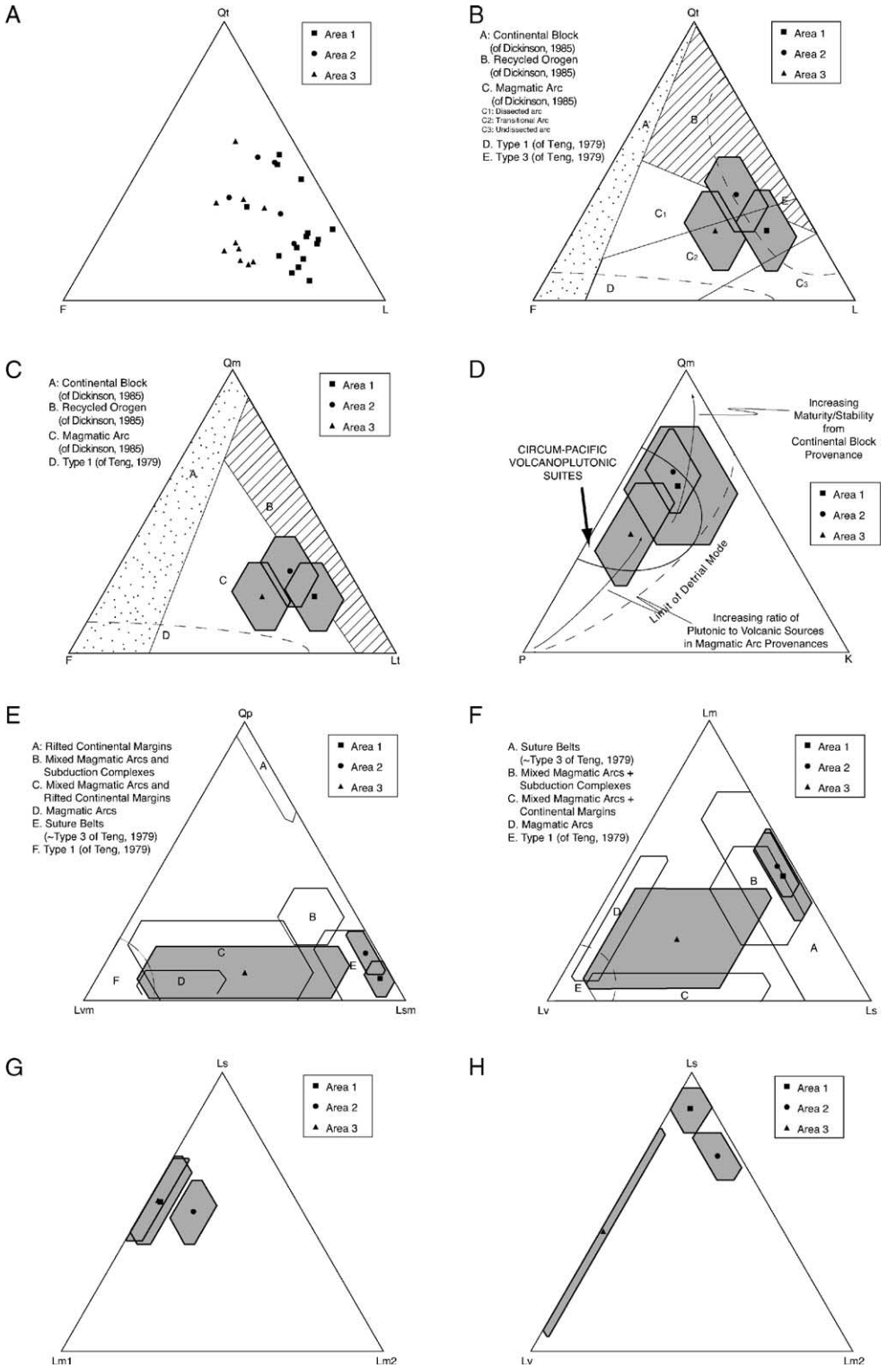

Fig. 3. (A) QtFL ternary diagram showing individual data points; (B) QtFL ternary diagram showing area means (mean detrital modes) and standard error polygons; (C) QmFLt ternary diagram showing area means and standard error polygons; (D) QmPK ternary diagram showing area means and standard error polygons; (E) QpLvmLsm ternary diagram showing area means and standard error polygons (Fields A, B, and C are defined by Ingersoll and Suczek, 1979); (F) LmLvLs ternary diagram showing area means and standard error polygons; (G) LsLm1Lm2 ternary diagram showing area means and standard error polygons (Dorsey, 1988); (H) LsLvLm2 ternary diagram showing area means and standard error polygons (this study).

Table 4
Total variance explained by the components extracted from area 1 sands

Component	Initial Eigenvalues			Extraction sums of squared loadings			Rotation sums of squared loadings		
	Total	% of variance	Cumulative %	Total	% of variance	Cumulative %	Total	% of variance	Cumulative %
1	12.920	86.134	86.134	12.920	86.134	86.134	7.241	48.270	48.270
2	1.112	7.410	93.545	1.112	7.410	93.545	6.791	45.274	93.545
3	.515	3.432	96.977						
4	.262	1.749	98.726						
5	.110	.733	99.459						
6	5.282e−02	.352	99.812						
7	1.778e−02	.119	99.930						
8	7.546e−03	5.030e−02	99.980						
9	1.460e−03	9.734e−03	99.990						
10	8.805e−04	5.870e−03	99.996						
11	4.116e−04	2.744e−03	99.999						
12	1.153e−04	7.685e−04	99.999						
13	6.229e−05	4.152e−04	100.000						
14	1.336e−05	8.909e−05	100.000						
15	3.319e−07	2.213e−06	100.000						

Extraction method: principal component analysis.

such as ridges and canyons. In order to shed light on relationships between sediment compositions and potential source terranes, principal component analysis was then applied independently to data sets corresponding to each of the three geographical domains defined earlier. Two components were extracted for each area. Tables 4, 5 and 6 list the total variance explained by the two components extracted for each area. The relationship between end-members and samples is shown in the rotated component matrices (Tables 7, 8 and 9). The factor scores that represent relationships between components and parameters are listed in Table 10. In area 1, first component shows high factor scores in most of the parameters contains Ls in the "denominator", strong negative factor scores with parameters that show metamorphic affinity (such as Lm_2, Lm_1, and Qp). Consequently, component 1 of area 1 yields an end-member of high sedimentary lithic fragment and low (negative) metamorphic lithic fragments (and Qp). On the other hand, the second component in area 1 yields an end-member of low sediment lithic fragments and high metamorphic lithic fragments. Notice the factor score on parameter K/F is low (small negative) on both components, which means K-spar is relatively unimportant in this area.

First component in area 2 yields an end-member with high percentage of low-grade metamorphic lithic fragment (Lm_1) and sedimentary lithic fragment (Ls), and strong negative contents of volcanic lithic fragment. Whereas second component show high sedimentary lithic fragment, monocrystalline quartz, and low metamorphic lithic fragments and low feldspar. First component of Area 3 show high factor score in volcanic lithic fragment, and the second component represents an end-member with moderate-high sedimentary lithic fragment.

4.3. Results from principal component analysis

The loadings of the first component serve to cluster the samples from area 1 into two groups. The loadings of one ranges from about 0.66 to approximately 0.89, and the other ranges from 0.36 to 0.56 (Table 7). The loadings of the second component in these two populations

Table 5
Total variance explained by the components extracted from area 2 sands

Component	Initial Eigenvalues			Extraction sums of squared loadings			Rotation sums of squared loadings		
	Total	% of variance	Cumulative %	Total	% of variance	Cumulative %	Total	% of variance	Cumulative %
1	4.472	89.436	89.436	4.472	89.436	89.436	2.434	48.678	48.678
2	.376	7.512	96.947	.376	7.512	96.947	2.413	48.269	96.947
3	.136	2.729	99.676						
4	1.071e−02	.214	99.890						
5	5.489e−03	.110	100.000						

Extraction method: principal component analysis.

Table 6
Total variance explained by the components extracted from area 3 sands

Component	Initial Eigenvalues			Extraction sums of squared loadings			Rotation sums of squared loadings		
	Total	% of variance	Cumulative %	Total	% of variance	Cumulative %	Total	% of variance	Cumulative %
1	6.259	56.902	56.902	6.259	56.902	56.902	5.745	52.230	52.230
2	3.594	32.673	89.575	3.594	32.673	89.575	4.108	37.345	89.575
3	.506	4.603	94.178						
4	.392	3.566	97.744						
5	.105	.956	98.700						
6	7.421e−02	.675	99.374						
7	3.520e−02	.320	99.694						
8	2.764e−02	.251	99.946						
9	3.446e−03	3.133e−02	99.977						
10	1.991e−03	1.810e−02	99.995						
11	5.518e−04	5.017e−03	100.000						

Extraction method: principal component analysis.

range from 0.70 to 0.91 and 0.38 to 0.60. (The *varimax* method we used to extract components leads to complementary component loadings, in that a sample with a high loading for the first component will have a low loading for the second component, and vice versa.) Samples JY10, JY12, and JY14 belong to the same core (Core OR487-13P); nevertheless, their properties are quite different. This phenomenon is less dramatic among samples taken from Core OR487-15P (JY16, JY17, JY18, JY20, and JY 23). The factor scores of component 1 show that it has a high correlation to sedimentary lithic fragments (and thus to total lithic fragments); the factor scores of component 2 show that it has high correlations to monocrystalline quartz (and so to total quartz) and low-grade metamorphic lithic fragments (and so to metamorphic lithic fragments).

Table 7
Rotated component scores of area 1 sands

	Component	
	1	2
JY10	.874	.451
JY12	.412	.812
JY136	.849	.378
JY14	.473	.806
JY16	.664	.740
JY17	.889	.421
JY18	.859	.431
JY20	.702	.702
JY23	.795	.597
JY28	.852	.454
JY32	.850	.416
319_17P	.356	.908
319_18P	.560	.801
319_19P	.379	.900
319_21P	.486	.850

Extraction method: principal component analysis.
Rotation method: varimax with Kaiser normalization.

The loadings of component 1 for sands from Cores 319-10P and 319-5P are rather low relative to other sands from area 2. The factor scores of component 1 are high for Lm, Lt (and so also L), Ls, and Lm_1. Component 2 is highly correlated to Qm (and so also to Qt).

Two obvious populations of component 1 loadings are observed in sands from area 3. One ranges from 0.99 to 0.88 and another from slightly negative to 0.14, with one sample (JY130) in between at 0.51. Samples JY95, JY106, JY109, and JY112 came from the same core OR487-28P, but the loading of JY95 for component 1 is low (actually slightly negative), whereas the other three sands analyzed from this core have very high loadings for component 1. The factor scores of component 1 are highly related to volcanic lithic fragments and plagioclase, whereas the factor scores of component 2 are correlated to sedimentary lithic fragments and monocrystalline quartz grains.

5. Interpretations

For the sands analyzed from offshore southern Taiwan, the modal average of area 1 sands plots in the provenance field of “recycled orogen” on a QmFLt

Table 8
Rotated component scores of area 2 sands

	Component	
	1	2
JY149	.730	.602
JY157	.923	.369
319_10P	.410	.909
319_15P	.495	.862
319_5P	.798	.588

Extraction method: principal component analysis.
Rotation method: varimax with Kaiser normalization.

Table 9
Rotated component scores of area 3 sands

	Component	
	1	2
JY100	.163	.933
JY106	.951	5.475e−02
JY109	.975	−7.242e−02
JY112	.881	.384
JY130	.513	.787
JY175	−5.570e−02	.889
JY78	.138	.922
JY95	−.111	.891
319_14P	.990	−1.902e−02
319_20P	.931	.141
319_6P	.971	8.744e−02

Extraction method: principal component analysis.
Rotation method: varimax with Kaiser normalization.

diagram, but well outside this field on the QtFL diagrams. Because the samples contain mainly fragments of slates, shales, and mudstones, it is clear that the major sediment source is the onland portion of the Taiwan orogen. This suggests that the provenance of sands deposited on the frontal accretionary prism (area 1 sands) is actually a "recycled orogen," perhaps more than an actual suture belt.

5.1. Sediment compositions offshore southern Taiwan

The modal average of sands from area 2, the complex suture zone, plots in the identical provenance field as area 1 sands in all ternary diagrams except the QtFL diagram, on which area 2 sands plot closer to the "recycled orogen" field than do area 1 sands (Fig. 3B). Because the composition of area 2 sands is similar to that of area 1, except for more abundant medium-grade metamorphic lithic fragments, and because the sediment source is also undoubtedly Taiwan, it is appropriate that area 2 sands should plot in the recycled-orogen provenance field. Again, these data suggest a broadening of the definition of this provenance field.

The modal average of sands from area 3 (the forearc basin and its western slope) contains abundant volcanic lithic fragments (nearly 50% of total lithic fragments are volcanic lithic fragments). On ternary diagrams, the mean detrital mode for area 3 sands plots in the magmatic arc provenance field, on both QtFL and QmFLt

Table 10
Factor scores of the components in each area

Variables	Area 1		Area 2		Area 3	
	FAC1	FAC2	FAC1	FAC2	FAC1	FAC2
K/F	−.40095	−.85805	−.67971	−.79011	−.83188	−.88598
$LsLm_1Lm\%Lm_1$	−.51981	1.28507	.85276	−.50083	.49272	.40880
$LsLm_1Lm_2\%Ls$	1.66804	−.38865	−.28943	1.64902	.80392	1.28829
$LsLm_1Lm_2\%Lm_2$	−.83518	−.48538	−.07168	−.76232	−.82631	−1.14385
$LsLvLm_1\%Lm_1$	−.65508	1.42821	1.39017	−.72598	−.85006	.40680
$LsLvLm_1\%Ls$	1.41837	−.17119	.25175	1.48203	−.67260	1.03911
$LsLvLm_1\%Lv$	−.45025	−.84597	−1.15026	−.37018	1.99300	−.89266
$LsLvLm_2\%Lm_2$	−.92801	−.24599	.66232	−1.01226	−.93618	−1.14982
$LsLvLm_2\%Ls$	1.59776	1.47264	.98837	1.67340	−.81970	2.34216
$LsLvLm_2\%Lv$	−.35671	−.81561	−1.15904	−.27527	2.22622	−.63909
LsLvLm%Lm	−.70456	1.59619	1.87371	−.61104	−.79856	.44252
LsLvLm%Ls	1.45876	−.32209	−.21096	1.39695	−.68803	1.01798
LsLvLm%Lv	−.44115	−.86305	−1.17109	−.40004	1.95693	−.90725
P/F	−.70258	−.81091	−1.08608	−.76424	−.97208	−1.17917
Qm/Qt	−.69290	−.80788	−1.08008	−.76151	−.97542	−1.17229
QmFLt%F	.04828	−.81843	−.02133	−.66236	.25594	−.13345
QmFL%Lt	1.35632	.56804	1.60135	−.03877	.81975	.73092
QmFLt%Qm	−1.09155	.66143	−1.08835	1.08700	−.60535	−.04423
QmPK%K	.59867	−1.19930	.06310	−.98696	−.60519	−.58340
QmPK%P	.50314	−.85105	.45505	−.90345	1.11175	.08188
QmPK%Qm	−.78877	2.46139	−.02649	2.27628	−.03623	1.05477
Qmu/Qm	−.70793	−.81151	−1.08740	−.77111	−.98332	−1.18854
QpLvLs%Ls	1.84410	1.03570	1.78734	.53105	.37278	2.03564
QPLvLs%Lv	−.44979	−.80293	−1.12710	−.36957	.95796	−.90972
QpLvLs%Qp	−1.08126	.17828	−.16858	.22440	−.86041	−.57268
QtFL%L	1.46162	.19310	1.39715	−.41641	.69363	.44921
QtFL%F	.04828	−.81843	−.02133	−.66236	.25594	−.13345
QtFL%Qt	−1.19685	1.03637	−.88415	1.46465	−.47923	.23749

diagrams, whereas on the QpLvmLsm diagram, it plots in the provenance field of "mixed magmatic arcs and rifted continental margins." This is satisfactory, given the geological setting of area 3 in a forearc basin (North Luzon Trough), adjacent to the Luzon arc, and the nature of the Taiwan orogen as uplifted and deformed rifted-margin sequences. However, on the LmLvLs diagram, the mean detrital mode for area 3 sands plots in the middle of the triangle, where no provenance field has previously been defined. Further investigation into individual samples shows two major compositional populations. One is composed of nearly pure volcanic detritus, with samples clustered very close to the volcanic lithic pole, whereas the other clusters close to the modal averages of sands from areas 1 and 2, dominated by sedimentary and metamorphic detritus; some area 3 sands plot in between these two end-members. This suggests that although most sediments came from a volcanic source (the Luzon arc immediately to the east), some sediments were derived from the west (the adjacent accretionary prism) or from Taiwan to the north, and sediment from these two sources generally remains distinct.

The fact that sands from all three areas have a Ls–Lm ratio of approximately 1:1 is interesting. The geological map of onland Taiwan shows that the ratio between the surface area of the western foredeep (made up mainly of sedimentary rock) and the area of the Central Range (exposing mainly low-grade metamorphic rocks) is roughly 3:2. Although medium-grade metamorphic rocks occupy some of the Central Range, the area is rather small. Chemical weathering and physical abrasion during transport from the source terranes on Taiwan to the depositional settings offshore Taiwan may preferentially break down a greater percentage of sedimentary lithic fragments relative to metamorphic lithic fragments, which may help explain the one-to-one ratio in the overall composition of offshore sands. One other possibility might be the difference in physiography (both the steepness of slopes and local relief) and possibly uplift rates between the western foredeep and the Central Range. The gentle slope in the western foredeep may result in less intense erosion, contributing relatively less detritus overall, whereas steeper and higher slopes in the Central Range may lead to more intense erosion and thus generate more clastic sediment.

The large amount of lithic fragments (53% on average) in this study is not surprising considering the collisional setting, characterized by rapid uplift (Liu and Yu, 1990) and fast erosion (Li, 1976; Willett et al., 2001). Rapid uplift, erosion, and sediment transport in this collisional setting prevents chemical weathering processes from significantly modifying detrital compositions, despite a tropical to subtropical setting with abundant rainfall and a humid climate. Abbott and Silver (1990) obtained a modal average of $Qt_{10}F_{21}L_{70}$ in sandstones from the Finisterre Mountains of northern Papua New Guinea, which is another modern example of an active arc-continent collision in a tropical setting.

5.2. "*Episodic depositions*" *and sediment dispersal paths*

Several cores are represented by more than one sand sample analyzed in this study. These include Cores OR487-10P, OR487-13P, OR487-14P, OR487-15P, and OR487-16P on the west side of accretionary prism, and Cores OR487-24P and OR487-28P in the North Luzon Trough. The detrital modes of these samples show that sand compositions are not consistent throughout individual piston cores. This is shown clearly by plots of these samples on ternary diagrams, especially using the LmLvLs and QpLvmLsm values (Table 3). With the longest cores at about 5 m in length and sampling intervals of generally less than 1 m, this result is somewhat unexpected. Further investigation using principal component analysis shows that the variability in the composition of sands within individual cores reflects significant fluctuations in sediment composition that probably reflect alternating sediment sources. In Core OR487-28P, four samples have been analyzed. Samples JY106, JY109, and JY112 have very high component loadings of 0.95, 0.98, and 0.85, respectively, for component 1, whereas the analogous component loading of sample JY95 is very low (-0.03). In Core OR487-28P (from the forearc basin), component 1 represents volcanic-source in composition and the second component represents the combination of sedimentary lithic fragments and monocrystalline quartz grains. Therefore, the higher component 1 loading represents more abundant volcanic lithic fragments, while lower component 1 loading means less abundant volcanic detritus and more abundant sedimentary lithic fragments. As the component loading indicates, sample JY95 contains considerably more sedimentary lithic fragments than the other three samples in the same core. This observation suggests that the sediment sources in this core are alternating in time, and because the samples are taken close to each other (and the sedimentation rate is likely high), this suggests that these sediment sources alternate on a short time scale. This feature is also observed in Cores OR487-13P, OR487-14P, OR487-15P, and OR487-16P, with two sediment sources alternating. This clearly

shows sediment input from different sources, and mixing of sediments of contrasting composition is common throughout the study area.

From the principal component analysis, the geographical trend shown by loadings of the second component in sands of the forearc basin (i.e., area 3; arc side of the accretionary prism) shows an increase toward the northwest and west, and a decrease toward the east and southeast. The loadings of the first component in area 3 sands are higher in the southeastern side of the basin and drop significantly toward the northern end of the basin. In sands from area 2 (complex suture zone), the loadings of the first component are higher toward the north, whereas loadings of the second component are higher toward the southwest. In sands from area 1 (frontal slope of the accretionary prism and adjacent South China Sea floor), loadings of the second component are higher toward the west and northwest and decrease toward the east, whereas the loadings of the first component show no obvious geographic trend.

5.3. Tectonic implications

Integrating modal analysis with geographic trends in composition from principal component analysis suggests several important points and implications for

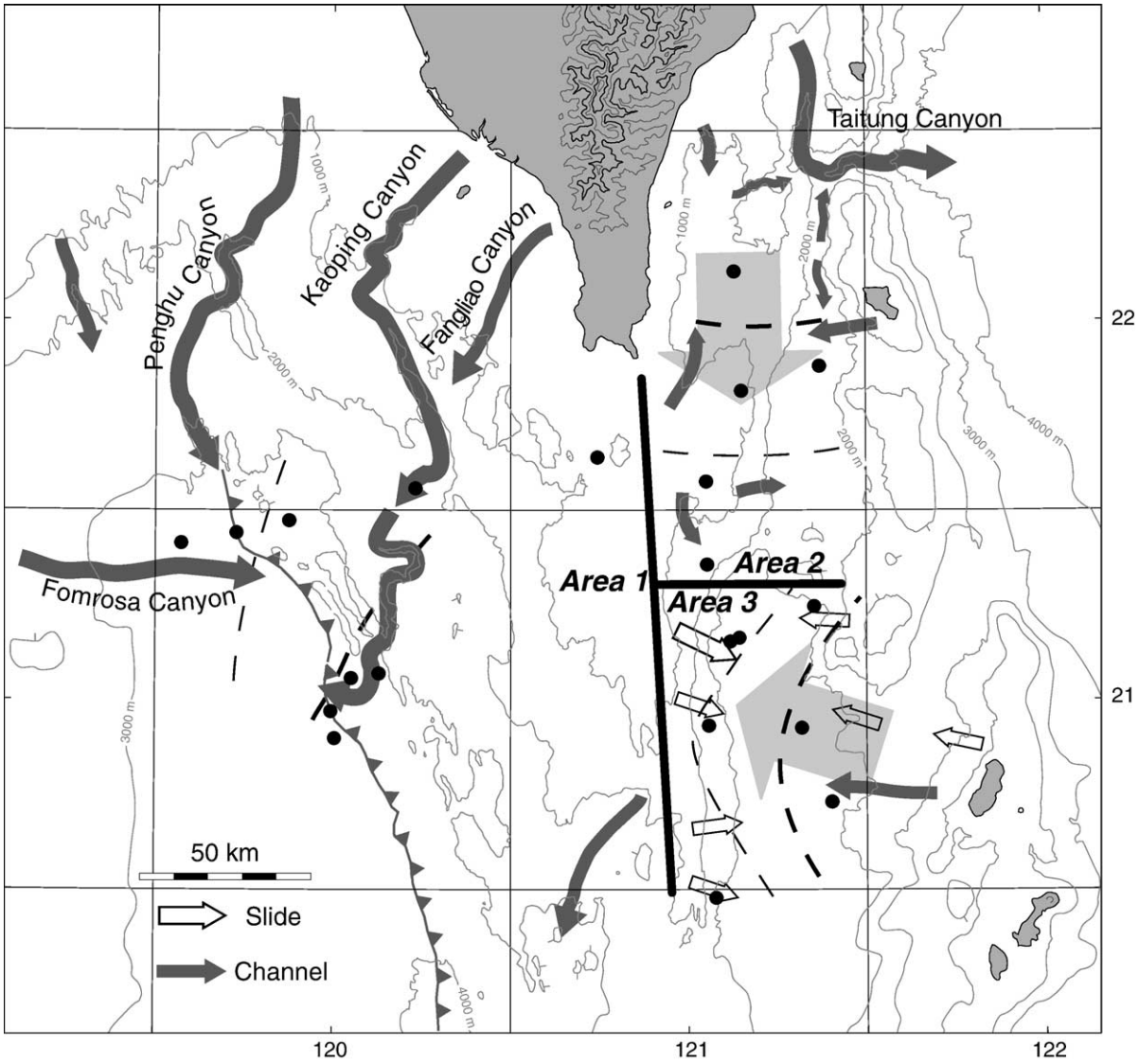

Fig. 4. Light grey arrows indicate the sediment dispersal paths indicated from component loadings of the first component using principal component analysis. Darker grey arrows are submarine canyons offshore southern Taiwan.

sedimentation in the modern collision zone south of Taiwan. First, depocenters in the forearc basin receive clastic input from the rear slope of the accretionary prism as well as the volcanic arc. Of the sands analyzed from the forearc basin region, most are dominated by volcanic lithic detritus; however, sands collected from Cores OR487-28P and OR487-24P are rich in sedimentary and metasedimentary lithic fragments, and these cores were taken in regions characterized as possible slide scars on the steep rear slope of the accretionary prism. Considering the analogous rock units exposed in the mature stage of the collision onland in Taiwan, this suggests that the process of submarine slides is important in the origin of stratigraphically chaotic mélanges. In particular, the apparent recycling of forearc-basin sands from the accretionary prism supports an olistostromal origin of the Lichi mélange (Huang et al., 1997; Page and Suppe, 1981).

Sediments analyzed in several regions cored show episodic input from contrasting sediment sources (Figs. 4 and 5). In area 1 sands, the major input of sand is from Taiwan, and a second sediment source appears to lie to the northwest (that is, the continental margin of China). It has long been speculated that sediments carried by major rivers of China should have important contribution in the sediment accumulation in the western Taiwan onshore and offshore. This result is the first indication of evidence of sedi-

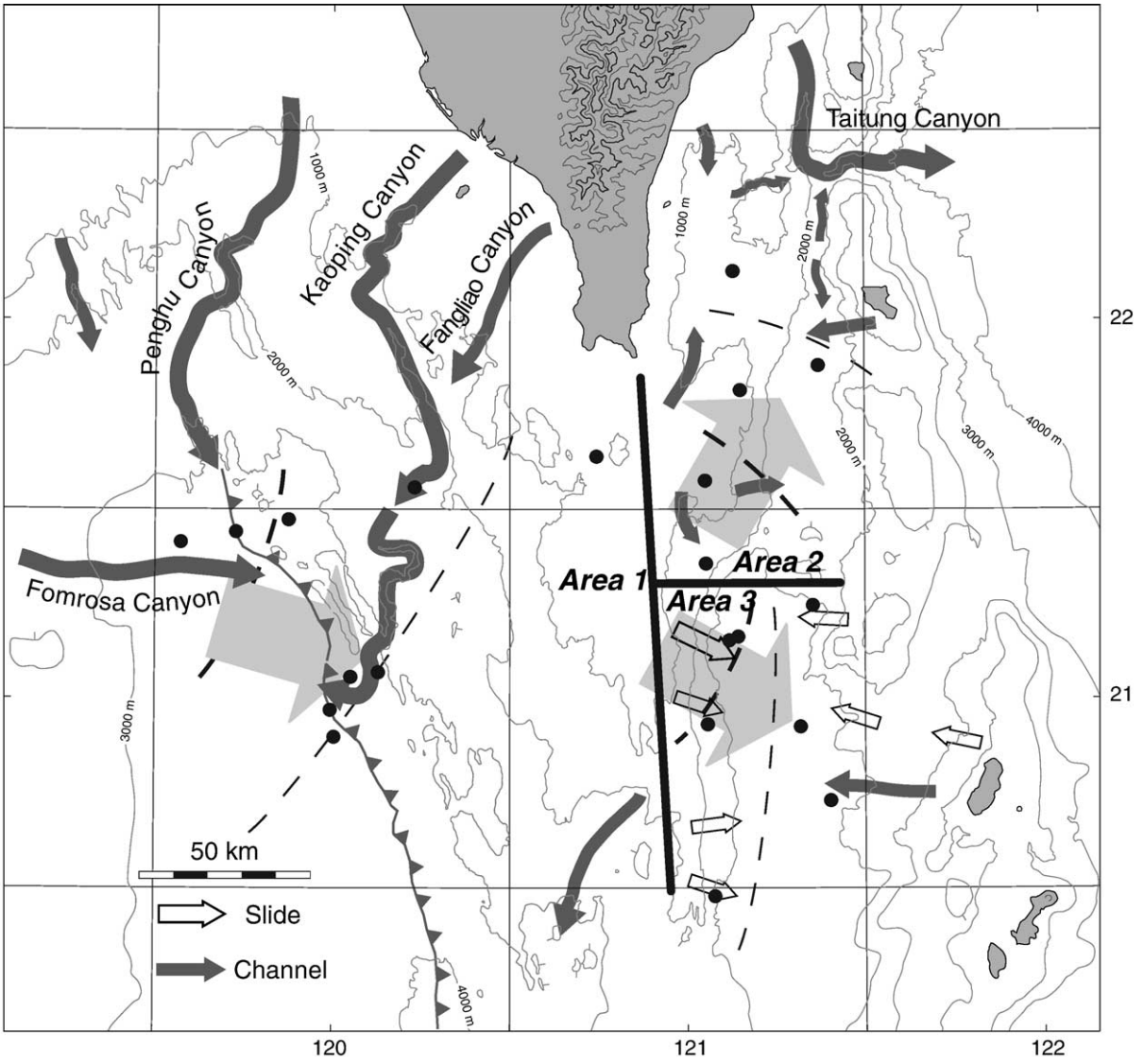

Fig. 5. Light grey arrows indicate the sediment dispersal paths indicated from component loadings of the second component using principal component analysis. Darker grey arrows are submarine canyons offshore southern Taiwan.

ment input from China. In area 3 sands, sediment is supplied mainly from southeast of the forearc basin, approximately coinciding with the location of the active volcanoes of the Batan islands; however, input of detritus from the accretionary prism is clearly observable through modal analysis as illustrated by ternary diagrams and through results of principal component analysis. The lack of medium-grade metamorphic detritus shows that sediment from eastern Taiwan does not enter this basin at present, as suggested by the detailed bathymetry. A major submarine canyon deflects southbound Taiwan-derived sediment toward the east, through the Luzon arc, and the North Luzon Trough is structurally closed at a latitude of 21°20′ (Lundberg et al., 1997). The sediment in this basin is mainly supplied by the volcanic island arc, and especially by the active arc segment southeast of the basin, plus episodic input of sediment from the accretionary prism that borders the basin to the west.

6. Conclusions

1. Sands deposited south of the island of Taiwan are lithic-rich, reflecting the ongoing arc-continent collision that has built Taiwan. The compositions of these sands serve to distinguish petrogenetic provinces in three distinct morphotectonic domains. These are (1) the frontal (western) slope of the submarine accretionary prism, plus the nearby seafloor of the incoming South China Sea; (2) the complex region north of the forearc basin, in which the suture zone is developing; and (3) the forearc basin and its immediate western slope, the rear slope of the accretionary prism.
2. Along the western slope of the accretionary prism, the major sediment input is from Taiwan, dominated by sedimentary lithic fragments and low-grade metamorphic lithic fragments. Minor but important amounts of sediment come from the northwestern side of this basin, suggesting that a second sediment source is southeastern China. This implies that sediment input from China is a significant component in the overall mass balance of the ongoing arc-continent collision.
3. Sands deposited in the North Luzon Trough (forearc basin) are dominated by volcanic lithic fragments derived from the east and southeastern side of the basin (the active volcanoes of the Batan islands), whereas minor components are fed episodically from the rear slope of the accretionary prism along the western side of the basin. This lends support to the olistostromal hypothesis for the origin of the Lichi Formation of eastern Taiwan, hypothesized to have formed in an analogous setting.
4. Individual piston cores in this area contain sands alternately rich in volcanic lithic fragments or sedimentary lithic fragments. This indicates that turbidites from different sources may remain distinct, alternating abruptly through time rather than being mixed by sediment transport and depositional processes.
5. Sands deposited in the Southern Longitudinal Trough and the adjacent basins have a major component derived from Taiwan to the north, but medium-grade metamorphic lithic fragments are less abundant than expected. This region is quite complex structurally and sedimentologically, however, and the present sampling density is insufficient to fully characterize surface processes here.
6. Refinement of provenance fields in the QtFL ternary diagram should be made to accommodate these new data from an active arc-continent collision zone. In particular, the field of “recycled orogen” provenance should be extended farther toward the lithic-fragment pole of the QtFL diagram.

Acknowledgements

We thank our shipboard colleagues M.-P. Chen, J.-P. Chi, J. Gieskes, C. Mahn, R. Vroom, and the captain and crew of the *R/V Ocean Researcher I* for very successful shipboard campaigns. M.-P. Chen has provided valuable ongoing collaboration and kindly facilitated our work on cores in Taipei. We thank C.S. Liu, C.Y. Huang, and D. Gerace for additional stimulating discussions. Supported by the National Science Foundation (Grant OCE-9618356); cruises OR-319 and OR-487 supported by the National Science Council of Taiwan.

References

Abbott, L.D., Silver, E.A., 1990. Northern Papua New Guinea: structure and sedimentation in a modern arc-continent collision. AAPG Bull. 74 (5), 594.

Abbott, L.D., Silver, E.A., Thompson, P.R., Filewicz, M.V., Schneider, C., 1994. Stratigraphic constraints on the development and timing of arc-continent collision in Northern Papua-New-Guinea. J. Sediment. Res., Sect. B Stratigr. Glob. Stud. 64 (2), 169–183.

Barr, T.D., Dahlen, F.A., 1990. Constraints on friction and stress in the Taiwan fold-and-thrust belt from heat-flow and geochronology. Geology 18 (2), 111–115.

Basu, A., 1976. Petrology of Holocene fluvial sand derived from Plutonic source rock: implications to paleoclimatic interpretation. J. Sediment. Petrol. 46 (3), 694–709.

Dickinson, W.R., 1970. Interpreting detrital modes of graywacke and arkose. J. Sediment. Petrol. 40 (2), 695–707.

Dickinson, W.R., 1985. Interpreting provenance relations from detrital modes of sandstones. In: Zuffa, G.G. (Ed.), Provenance of Arenites. D. Reidel Publishing Company, Holland, pp. 333–361.

Dickinson, W.R., Suczek, C.J., 1979. Plate tectonics and sand composition. AAPG Bull. 63, 2164–2182.

Dorsey, R.J., 1988. Provenance evolution and unroofing history of a modern arc-continent collision—evidence from petrography of Plio-Pleistocene sandstones, eastern Taiwan. J. Sediment. Petrol. 58 (2), 208–218.

Ernst, W.G., 1983. Mineral paragenesis in metamorphic rocks exposed along Tailuko Gorge, Central Mountain Range, Taiwan. J. Metamorph. Geol. 1, 305–329.

Findlay, R.H., Abbott, L.D., Silver, E.A., Thompson, P.R., Filewicz, M.V., Schneider, C., Abdoerrias, C., 1995. Stratigraphic constraints on the development and timing of arc-continent collision in northern Papua New Guinea [discussion and reply]. J. Sediment. Res., Sect. B Stratigr. Glob. Stud. 65 (2), 281–286.

Graham, S.A., Ingersoll, R.V., Dickinson, W.R., 1976. Common provenance for lithic grains in Carboniferous sandstones from Ouachita Mountains and Black Warrior Basin. J. Sediment. Petrol. 46, 620–632.

Hiscott, R.N., Pickering, K.T., Beeden, D.R., 1986. Progressive filling of a confined Middle Ordovician foreland basin associated with the Taconic Orogeny, Quebec, Canada. In: Allen, P.A., Homewood, P. (Ed.), Foreland Basins: Special Publication of the International Association of the Sedimentologist, vol. 8.

Ho, C.S., 1982. Tectonic Evolution of Taiwan: Explain Text of the Tectonic Map of Taiwan: Taipei. The Ministry of Economic Affairs, Republic of China. 126 pp.

Huang, C.Y., Shyu, C.T., Lin, S.B., Lee, T.Q., Sheu, D.D., 1992. Marine geology in the arc continent collision zone off southeastern Taiwan—implications for Late Neogene evolution of the Coastal Range. Mar. Geol. 107 (3), 183–212.

Huang, C.Y., Wu, W.Y., Chang, C.P., Tsao, S., Yuan, P.B., Lin, C.W., Xia, K.Y., 1997. Tectonic evolution of accretionary prism in the arc-continent collision terrane of Taiwan. Tectonophysics 281 (1–2), 31–51.

Ingersoll, R.V., 1988. Tectonics of sedimentary basins. Geol. Soc. Amer. Bull. 100, 1704–1719 (November).

Ingersoll, R.V., 1990. Actualistic sandstone petrofacies: discriminating modern and ancient source rocks. Geology 18, 733–736 (August).

Ingersoll, R.V., Suczek, C.A., 1979. Petrology and provenance of Neogene sand from Nicobar and Bengal Fans, DSDP sites 211 and 218. J. Sediment. Petrol. 49, 1228–1271.

Ingersoll, R.V., Bullard, T.F., Ford, R.L., Grimm, J.P., Pickle, J.D., Sares, S.W., 1984. The effect of grain size on detrital modes: a test of the Gazzi-Dickinson point-counting method. J. Sediment. Petrol. 54 (1), 0103–0116.

Johnsson, M.J., Stallard, R.F., Lundberg, N., 1991. Controls on the composition of fluvial sands from a tropical weathering environment—sands of the Orinoco River Drainage-Basin, Venezuela and Colombia. Geol. Soc. Amer. Bull. 103 (12), 1622–1647.

Lash, G.G., 1987. Longitudinal petrographic variations in a Middle Ordovician trench deposit, central Appalachian Orogen. Sedimentology 34, 227–235.

Li, Y.-H., 1976. Denudation of Taiwan island since the Pliocene Epoch. Geology, 105–107 (FEB.).

Liew, P.M., Hsieh, M.L., Shyu, B.H., 2004. An overview of coastal development in a Young Mountain Belt-Taiwan. Quat. Int. 115, 39–45.

Liu, T.K., 1982. Tectonic implications of fission track ages from the Central Range, Taiwan. Geol. Soc. China Proc. 25, 22–37.

Liu, C.-C., Yu, S.-B., 1990. Vertical crustal movements in eastern Taiwan and their tectonic implication. Tectonophysics 183, 111–119.

Lundberg, N., Dorsey, R.J., 1988. Synorogenic sedimentation and subsidence in a Plio-Pleistocene collisional basin, Eastern Taiwan. In: Kleinspehn, K.L., Paola, C. (Eds.), New Perspectives in Basin Analysis. Springer-Verlag, New York, pp. 265–280.

Lundberg, N., Dorsey, R.J., 1990. Rapid Quaternary emergence, uplift, and denudation of the Coastal Range, eastern Taiwan. Geology 18, 638–641.

Lundberg, N., Reed, D.L., Liu, C.S., Lieske, J., 1997. Forearc-basin closure and arc accretion in the submarine suture zone south of Taiwan. Tectonophysics 274 (1–3), 5–23.

Page, B.M., Suppe, J., 1981. The Pliocene Lichi Melange of Taiwan—its plate-tectonic and olistostromal origin. Am. J. Sci. 281 (3), 193.

Peng, T.H., Li, Y.H., Wu, F.T., 1977. Tectonic uplift of the Taiwan island since the early Holocene. In: Ho, C.S. (Ed.), Biq Ching-chang Dedicational Volume, Geological Society of China Memoir, pp. 57–69.

Sibuet, J.C., Hsu, S.K., 2004. How was Taiwan created? Tectonophysics 3791 (4), 159–181.

Suppe, J., 1984. Kinematics of arc-continent collision, flipping of subduction, and back-arc spreading near Taiwan. Mem. Geol. Soc. China 6, 21–33.

Suttner, L.J., Basu, A., 1985. The effect of grain size on detrital modes: a test of the Gazzi-Dickinson point-counting method—discussion. J. Sediment. Petrol. 55 (4), 0616–0627.

Teng, L.S., 1979. Petrographical study of Neogene sandstones of the Coastal Range, eastern Taiwan (1. Northern Part). Acta Geol. Taiwanica 20, 129–155.

Teng, L.S., 1990. Geotectonic evolution of late Cenozoic arc-continent collision in Taiwan. Tectonophysics 183, 57–76.

Teng, L.S., 1996. Extensional collapse of the northern Taiwan mountain belt. Geology 24 (10), 949–952.

Uddin, A., Lundberg, N., 2004. Miocene sedimentation and subsidence during continent–continent collision, Bengal Basin, Bangladesh. Sediment. Geol. 164 (1–2), 131–146.

Wang, C.H., Liew, P.M., Liu, T.K., Burnett, W.C., 1989. The Holocene uplift rates on both sides of the active plate–collision boundary in Taiwan. Eos (Transactions American Geophysical Union) 70, 403.

Willett, S.D., Fisher, D., Yeh, E.-C., Anonymous, 2001. High Erosion Rates in Taiwan from Apatite and Zircon Fission Track Ages.